



Advanced ultrasound in the diagnosis of prostate cancer

Jean-Michel Correas¹ · Ethan J. Halpern² · Richard G. Barr³ · Sangeet Ghai⁴ · Jochen Walz⁵ · Sylvain Bodard¹ · Charles Dariane⁶ · Jean de la Rosette⁷

Received: 23 March 2020 / Accepted: 30 March 2020 / Published online: 18 April 2020
© Springer-Verlag GmbH Germany, part of Springer Nature 2020

Abstract

The diagnosis of prostate cancer (PCa) can be challenging due to the limited performance of current diagnostic tests, including PSA, digital rectal examination and transrectal conventional US. Multiparametric MRI has improved PCa diagnosis and is recommended prior to biopsy; however, mp-MRI does miss a substantial number of PCa. Advanced US modalities include transrectal prostate elastography and contrast-enhanced US, as well as improved B-mode, micro-US and micro-Doppler techniques. These techniques can be combined to define a novel US approach, multiparametric US (mp-US). Mp-US improves PCa diagnosis but is not sufficiently accurate to obviate the utility of mp-MRI. Mp-US using advanced techniques and mp-MRI provide complementary information which will become even more important in the era of focal therapy, where precise identification of PCa location is needed.

Keywords Prostate cancer diagnosis · Micro-ultrasound · mp-MRI · mp-US · Prostate US elastography · Contrast-enhanced US · Fusion imaging · Prostate biopsy · Dispersion imaging

Introduction

Prostate cancer (PCa) is the most common visceral cancer diagnosed in men. It is a public health issue in most Northern and Western countries with an incidence above 200 per 100,000 men per year. The high incidence of PCa is related to aging of population, exogenous factors such as metabolic

syndrome, improved sensitivity of diagnostic techniques and screening with Prostatic-Specific Antigen (PSA) [1]. Despite early diagnosis secondary to improvements in imaging techniques, increased use of PSA testing and more efficient treatments, PCa-specific mortality rate has declined only slightly (– 2.5% per year for the period 2000–2005). PCa management is limited by lack of identified risk factors, lack of an efficient systematic screening test and prognostic factors, as well as by the limited specificity of diagnostic examinations. The disease is also complex, heterogeneous and multifocal, with underdiagnosis or overdiagnosis issues and a prolonged clinical course requiring an outcomes evaluation period of over 10 years.

PCa diagnostic limitations

Diagnostic limitations include limited diagnostic performance of Digital Rectal Examination (DRE), interindividual variation in PSA levels and lack of sensitivity of conventional TransRectal Ultrasound (TRUS). Systematic PSA screening for PCa is not recommended and remains a controversial topic due to the lack of demonstrated impact on overall survival or cancer-specific survival, as well as the risks of overdiagnosis and overtreatment [2]. The benefits

✉ Jean-Michel Correas
jean-michel.correas@aphp.fr

¹ Department of Adult Radiology, Paris University and Necker University Hospital, 149 rue de Sèvres, 75015 Paris Cedex 15, France

² Department of Radiology, Thomas Jefferson University, Philadelphia, PA, USA

³ Department of Radiology, Northeastern Ohio Medical University, Rootstown, OH, USA

⁴ Department of Medical Imaging, Princess Margaret Cancer Centre and University of Toronto, Toronto, ON, Canada

⁵ Department of Urology, Institut Paoli-Calmettes Cancer Centre, Marseille, France

⁶ Department of Urology, Paris University and European Hospital Georges Pompidou, Paris, France

⁷ Department of Urology, Istanbul Medipol University, Istanbul, Turkey

of any proposed diagnostic approach need to outweigh its drawbacks, which include complications related to treatment (urinary incontinence, impotence, radiation cystitis or proctitis), to diagnostic methods (post-biopsy prostatitis, hematuria, rectal hemorrhage, retention, pain, complications due to Magnetic Resonance Imaging (MRI) and administration of contrast agents), to psychological impact of this diagnosis and finally to the downstream costs of false-positive PSA and MRI tests. Individual screening is now recommended in targeted populations at high PCa risk and in non-targeted males over 50 who desire screening after disclosure of the benefits and risks. New tests such as Prostate Health Index, 4Kscore test, Prognostic PCA3, or ProMark depends may provide greater diagnostic accuracy but remain to be evaluated for screening [3].

PCa may be suspected when the PSA level is abnormal or increasing, or if DRE is abnormal. Further tests are then carried out, starting with TRUS examination followed in most cases by a TRUS-guided biopsy. A multi-parametric MRI (mp-MRI) is now recommended prior to prostate biopsy to increase the detection rate particularly for anterior lesions. Prostate biopsy also allows estimation of tumor volume (number and spatial dispersion of the positive cores, tumor length in each positive sample) and aggressiveness (Gleason Score (GS) and invasion of the capsule or the neurovascular bundles). However, PCa screening using PSA has several limitations, including substantial number of unnecessary biopsies in patients with no cancer or with indolent cancer that will not benefit from immediate treatment, with an estimated over-Detection Rate (DR) ranging from 27 to 56% [4]. The false-negative rate of systematic prostate biopsy varies from 17 to 21%, in patients with a negative first series of biopsies [5, 6]. Increasing in the number of core biopsies (saturation biopsies up to 40) improves PCa detection and offers a better estimation of the tumor volume and GS [7, 8], but has many limitations including increased cost and morbidity, and over-diagnosis and overtreatment of microscopic tumor foci [9]; furthermore, a negative saturation biopsy does not truly rule out PCa [7, 8].

Mp-MRI, combining T2-weighted imaging and functional sequences, has attracted significant interest for tumor detection and staging [10–12]. Use of mp-MRI in the biopsy naive population may obviate the need for biopsy in > 20% of the patients, though the reported negative predictive value of mp-MRI for clinically significant PCa (cs-PCa) is about 85% [13, 14]. However, MRI performance varies with the combination of positive features that is selected for cancer diagnosis as well as the acquisition parameters (T2-weighted imaging, diffusion sequences including ADC calculation, dynamic contrast-enhanced imaging and sometimes spectral MRI). While the sensitivity of MRI is high for large (> 1 cm³) and higher grade PCa (> Gleason Grade 1), it remains low for the detection of smaller lesions of limited

GS (≤ 6) and there is little information to help distinguish between aggressive and indolent tumors [15–17]. Use of PIRADS v2.1 and computer-aided diagnosis systems may help in standardizing the interpretation of images and in defining thresholds for distinguishing aggressive tumors [18, 19]. MRI may be limited in patients with non-compatible pacemakers, non-compatible stents and grafts (particularly at higher field strength of 3 and 7 T), patients with claustrophobia or pelvic metal (hip replacement surgery, pelvic orthopedic metal work).

Conventional TRUS B-mode imaging has been studied extensively to assess its performance for PCa diagnosis. However, the sensitivity and specificity of conventional TRUS are limited ranging between 40 and 50% for PCa detection, with minimal additional improvement using Color/Power Doppler [20–22].

PCa is typically stiffer than the surrounding normal prostate parenchyma, and this feature is routinely used for DRE [23]. However, DRE diagnostic capabilities remain limited as this exam is highly subjective, with large inter-observer variability. DRE is not an accurate method for staging PCa and locating PCa foci, two important factors for planning treatment [24, 25]. An imaging technique able to map tissue elasticity—prostate trans-rectal US elastography would be useful in detecting PCa and characterizing focal areas of abnormal signals.

Conventional prostate TRUS imaging improvements

The limitations of B-mode imaging in identifying PCa result from two main factors: the similar backscatter signals from PCa and normal prostate parenchyma and the heterogeneity of the transition zone. Nonlinear imaging (or Tissue Harmonic Imaging) has been implemented in most high-end US imaging system. An ultrasound pulse is transmitted at a fundamental frequency and a harmonic response is generated by the nonlinear propagation of the ultrasound pulse in the tissue (typically at double the central transmit frequency, explaining the name “second harmonic imaging”). The major advantages of nonlinear imaging are improved contrast resolution and reduced clutter (noise) due to lower ultrasound aberrations present at second harmonic (Fig. 1a, b). However, the use of higher frequency results in attenuation artifacts, particularly when prostate calcifications are present. Spatial compound imaging is another technique that can be combined with nonlinear imaging to improve contrast resolution and reduce clutter and speckle. Pulses can be steered at different angles (typically 3–5 angles), so that tissue interfaces are visualized from various views, improving structure delineation and identification (Fig. 1c, d). Additional filtering techniques can be combined to improve

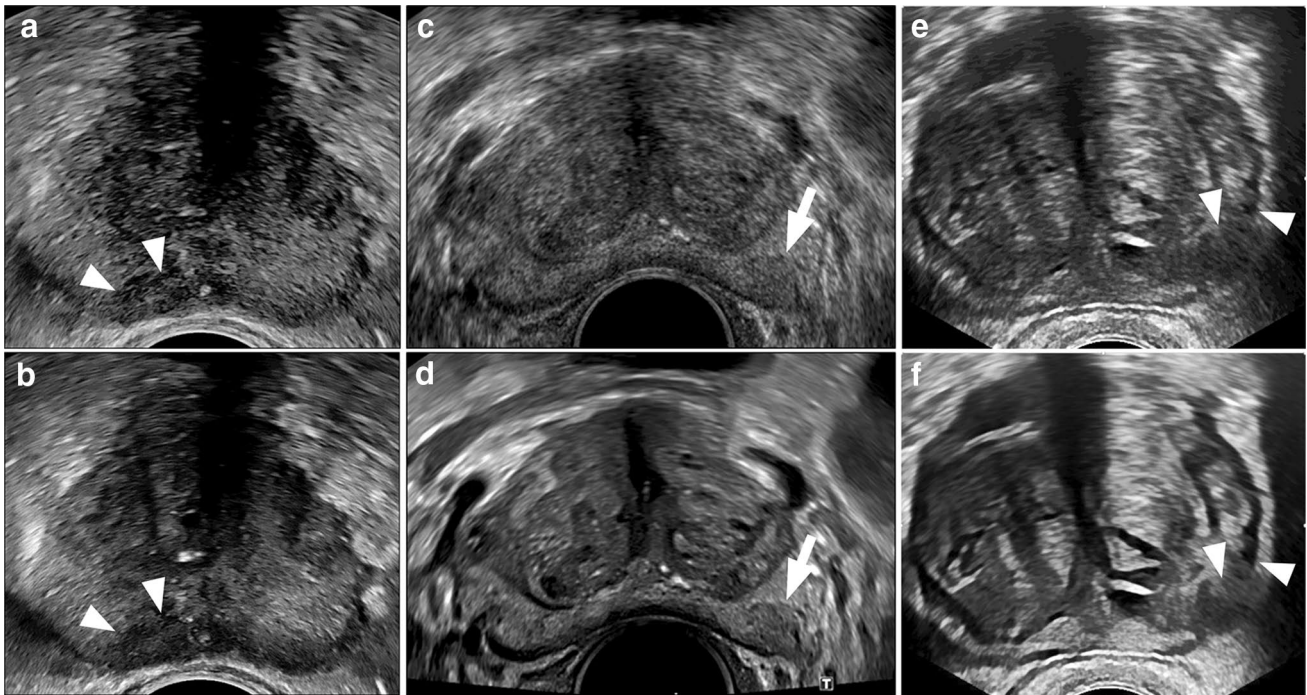


Fig. 1 Conventional B-mode imaging improvements. **a, b** Non-linear imaging (also called Tissue Harmonic Imaging) improves contrast resolution and reduces clutter as seen on **b** in comparison to conventional B-mode imaging (**a**), resulting in better visualization of PCa (arrow heads). **c, d** Compounding imaging also improves contrast resolution and PCa detection (arrow) as seen on **d**, in comparison to

conventional B-mode imaging (**c**). **e, f** Additional filtering techniques, such as carving filtering (Hitachi MS), can be combined to improve PCa detection as seen on **f**, in comparison to conventional B-mode imaging (**e**). Note that capsule conspicuity and extracapsular extension of PCa is better visualized (arrow)

the detection of prostate nodules, such as carving filtering (Hitachi MS) (Fig. 1e, f).

The shape and frequency of the transrectal transducer play a key role. Linear arrays are typically designed with higher frequency to provide higher spatial and contrast resolution. However, higher transmit frequency is associated with increased attenuation (about 1 dB per MHz, keeping in mind that a 3-MHz increase in frequency results in twice attenuation of the US beam). Micro-convex arrays require more interpolation in between lines forming the images and typically provide lower spatial resolution than linear arrays. They can be located at the tip of the transducer (end-fire probes) or proximal to the tip of the probe, as in bi-plane transducers. Over the past decade, the tendency for diagnostic prostate ultrasound has been to increase the central frequency, reaching 7–9 MHz, using broadband single-crystal piezoelectric elements.

Recently, the concept of ultrasound biomicroscopy developed at the Sunnybrook Health Science Centre by S Foster et al. was extended to prostate ultrasound imaging [26]. Prostate micro-ultrasonography is performed at frequencies ranging between 14 and 29 MHz. Theoretical spatial resolution at this frequency is between 50 and 70 μm [27]. The prostate anatomy can be redefined, with identification of anatomic

details usually not seen in conventional US examinations (Fig. 2). The system allows detection of additional focal lesions that requires stratification based on a PCa risk score called PRI-MUS [27]. Published studies from individual centers report an increase in PCa detection rate (up to 94%) and Area Under the Curve between 0.60 and 0.80 [27–29]. Micro-ultrasonography allows US real-time guided biopsy of even small suspicious nodules. In a recent meta-analysis based on 769 patients, micro-ultrasound pooled sensitivity, specificity, diagnostic odds ratio, and areas under the summary receiver operating characteristic curve were 0.91, 0.49, 10, and 0.82, respectively [30]. While micro-ultrasound is a promising new imaging device which has the potential of improving sensitivity of TRUS prostate biopsy, larger multi-center trials are awaited to establish its role in PCa detection and determine whether micro-ultrasound will improve the detection of cs-PCa without resulting in an increased number of biopsies directed toward newly visible benign nodules. Initial studies have demonstrated that micro-ultrasound is able to visualize MRI targets in real time, rather than relying on MRI–TRUS fusion software coupled with conventional TRUS for targeting [26]. Micro-ultrasound, therefore, may have the potential to enhance accuracy of mp-MRI in detecting cs-PCa.

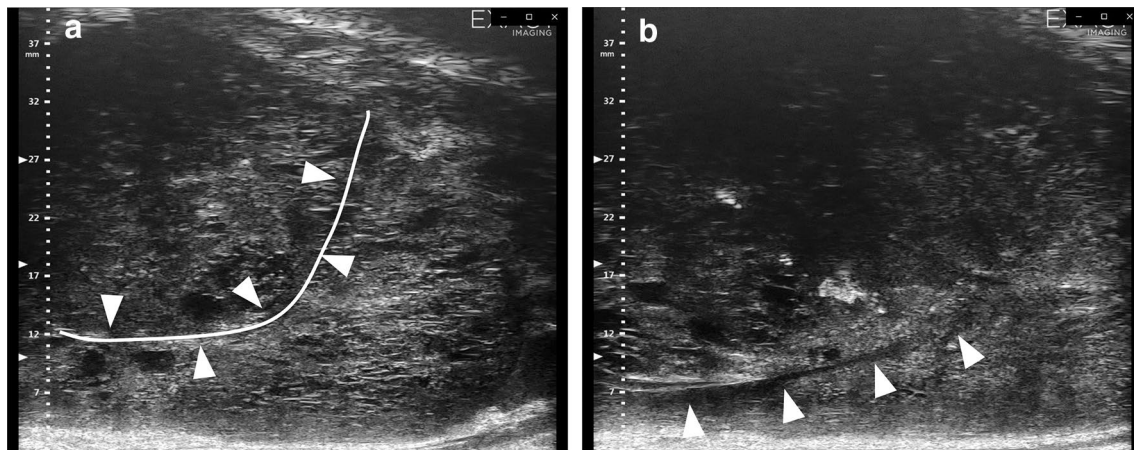


Fig. 2 Prostate micro-ultrasonography at 14–29 MHz: improved anatomy assessment. **a** The distinction between peripheral and transition zone at the apex is clearly identified. **b** The ejaculatory duct at the base is easily followed. Note US attenuation due to the use of higher frequency

B-mode data can be processed using various algorithms to increase PCa detection. Preliminary results performed with Computerized Trans-rectal US, alone or combined with MRI, can improve PCa detection in high-risk patients [27, 28]. Histoscanning is based on raw data statistical analysis of tissue characteristics and initial results with this technique were encouraging [29, 30]. However, recent publications revealed limited diagnostic performance with sensitivity ranging from 12.1 to 20.7% and positive predictive values ranging from 17.4 to 33.3%, as well as a lack of consistent results [31, 32]. Computerized interpretation of TRUS may be positively impacted by Artificial Intelligence with deep learning algorithms, an approach which is different from earlier Computer-Assisted Diagnostic systems [33].

Conventional Color-Doppler Ultrasound (CDUS) can increase PCa detection rate when biopsy samples are taken on hypervascular areas, despite normal B-mode appearance [22]. Of course, settings should be adapted to low signal intensity and slow flow detection, and compression of the prostate peripheral zone by the transducer should be avoided as much as possible. Conventional power Doppler imaging (with or without directional information) exhibits a slightly better sensitivity as compared with color Doppler. Recently, micro-Doppler imaging techniques have been introduced using adaptive algorithms to eliminate motion artifacts, and with a higher number of pulses dedicated to flow encoding (such as Superb MicroFlow Imaging™ SMI) (Fig. 3). Preliminary results are encouraging with positive correlation between microvasculature detected by SMI and GS [31]. Micro-Doppler imaging can be performed at high mechanical index, or at low acoustic power after ultrasound contrast agent administration. Bubble trace can then be accumulated by temporal summation of the signals (Fig. 4).

Prostate TRUS elastography

Conventional imaging techniques do not provide information about in vivo prostatic elastic properties. PCa tissue is stiffer than surrounding healthy prostate tissue due to several changes including increased cellular density and micro-vascularization, destruction of glandular architecture and development of stromal reaction combined with collagen deposition in the surrounding prostate parenchyma [34–37]. Ex vivo studies of tissue samples demonstrate a significant difference between normal and cancerous prostate tissue stiffness [38–42]. Moreover, this increase in tissue stiffness was correlated with GS [41] and disease severity [42]. The stiffness of benign prostatic hyperplasia (BPH) nodule is also significantly different from that of PCa nodules [38, 42].

Prostate elastography should be performed after a complete B-mode and color-Doppler examination conducted in transverse and sagittal planes, to measure prostate volume, identify suspicious areas in the peripheral gland (mostly hypoechoic and/or hypervascular) and analyze the periprostatic space (including the seminal vesicles) [43]. Several ultrasound-based methods have been developed to measure in vivo prostate tissue elasticity and provide elasticity maps. Elastography may improve both lesion characterization and PCa detection, as stiff lesions not visible at conventional TRUS imaging may be detected on elastograms. Two different approaches have been developed: (1) the analysis of the strain or deformation of a tissue during a mechanical stress (static/quasi-static elastography or strain elastography) and (2) the analysis of the propagation speed of a shear wave (SW) which is linked to tissue elasticity. Both techniques require significant training to obtain appropriate and reproducible elastograms [43].

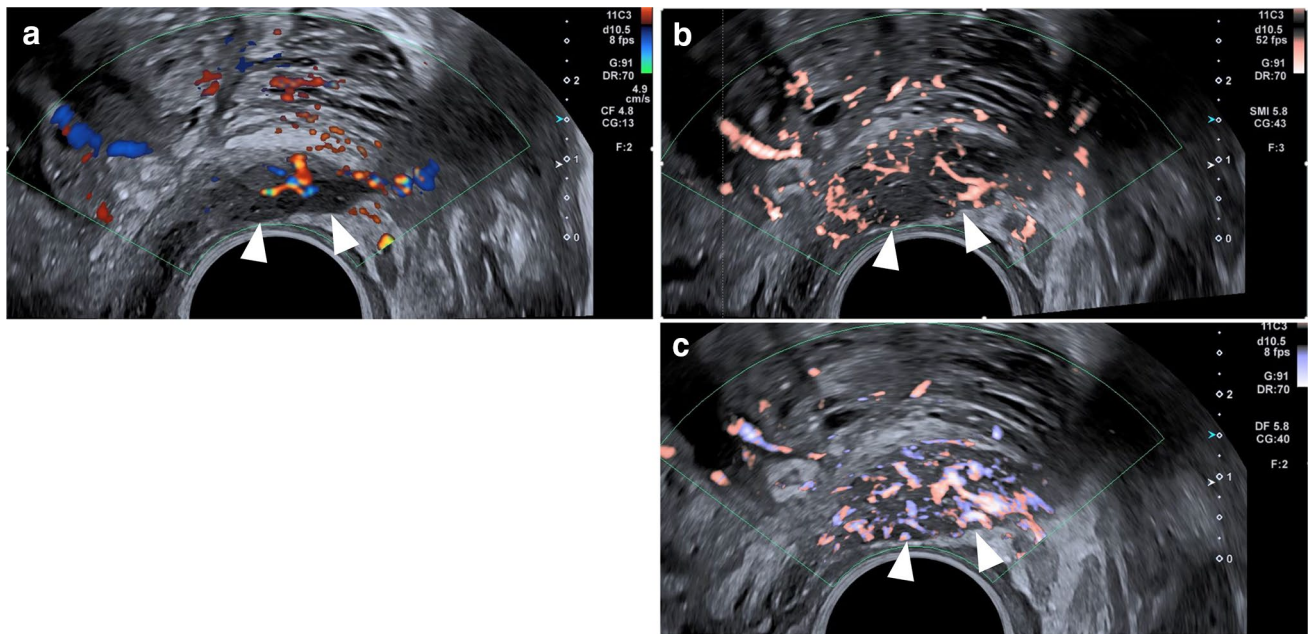


Fig. 3 Conventional color-Doppler imaging improvements. **a** Some abnormal blood flow disturbance is detected inside this hypoechoic nodule corresponding to high-grade PCa. **b**, **c** micro-Doppler techniques (such as Superb MicroFlow Imaging–SMI™ (**b**) and

Advanced Dynamic Flow–ADF™ (**c**) Canon MS) improve the detection of tumor vascularity due to better sensitivity and spatial resolution

Strain elastography (SE)

Prostate strain elastography requires application of alternate compression and decompression cycles through the rectal wall using the endocavitary transducer as a compression device. Speckle comparison between each cycle allows calculation of a color-coded map, called the elastogram, overlaid on the B-mode image. There are specific technical issues which require attention during SE due to the micro-convex shape of end-fire transducers for compression and decompression. To generate useful elastograms without artifact, the deformation should be homogeneous over the entire imaging plane and should not displace the prostate. A water-filled balloon placed between the imaging probe and the rectal wall may improve deformation homogeneity, but is not frequently used in practice [44]. A quality index has been developed to ensure appropriate speed of the compression/decompression cycle and amount of pressure applied. The position of the strain box is another issue as the stiffness color scale is automatically distributed from the lowest to the highest strain found in that region-of-interest (ROI). This ROI should cover the entire gland and the surrounding tissues to reduce artifactual variation of the displayed strain. Moreover, SE does not provide true quantitative information. The value of semi-quantitative information that can be derived by measuring strain ratio between two regions of interest (usually one considered “normal” in terms of stiffness and one considered “abnormal”) remains limited.

However, this technique is easy to use and has become available on many endocavitary transducers to allow prostate SE imaging. A quality index has been developed to ensure appropriate speed of compression and pressure amount.

Using SE, stiff tissues with low strain may be highlighted by color coding in blue, while soft tissues with high strain are color coded in red (but other color maps may be used). The normal strain elastography pattern of the peripheral zone is of intermediate elasticity; while, the inner gland (mostly the transitional zone) shows more heterogeneity related to BPH, and increasing stiffness with greater age and volume [45]. Hypoechoic lesions coded in blue are highly suspicious to be malignant (Fig. 5).

Prostate SE improves both characterization of focal lesions and detection of PCa compared to B-mode US. SE PCa detection rate depends on tumor size volume and localization, as well as Gleason score and extra-capsular extension [44, 46–49]. The meta-analysis performed by Zhang et al. on 508 patients demonstrated a pooled sensitivity of 0.72 (95% confidence interval: 0.70–0.74) and a pooled specificity of 0.76 (0.74–0.78), respectively, with an area under the curve of 0.841 ($Q^* = 0.773$) [50]. However, benign lesions, particularly inflammatory lesions [51], also exhibit higher stiffness, reducing the positive predictive value to 39% in men with PSA lower than 4 ng/mL [52]. SE cancer detection compared to radical prostatectomy ranges from 49 to 87% for sensitivity, and 60–92% for specificity, with accuracy varying from 62 to 92%, compared with B-mode

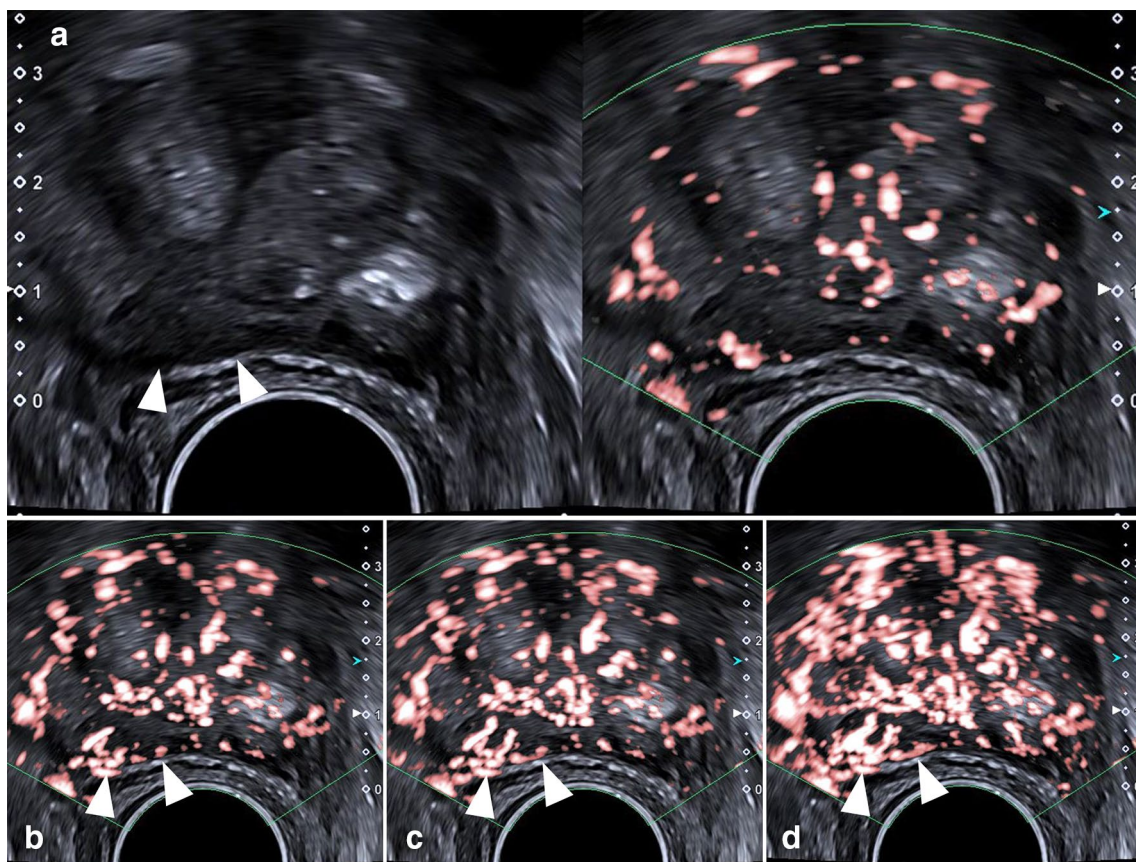


Fig. 4 Contrast-enhanced SMI™ using MicroFlow imaging (temporal summation of the signals). **a** Micro-Doppler imaging can be performed at low acoustic power after UCA administration (PCa is shown with arrow heads). **b–d** Each bubble trace can be accumulated

with a technique similar to the Maximum Intensity Projection used at CT, improving the identification of all micro vessels. In a few seconds, PCa abnormal vascularity pattern is identified (arrow heads)

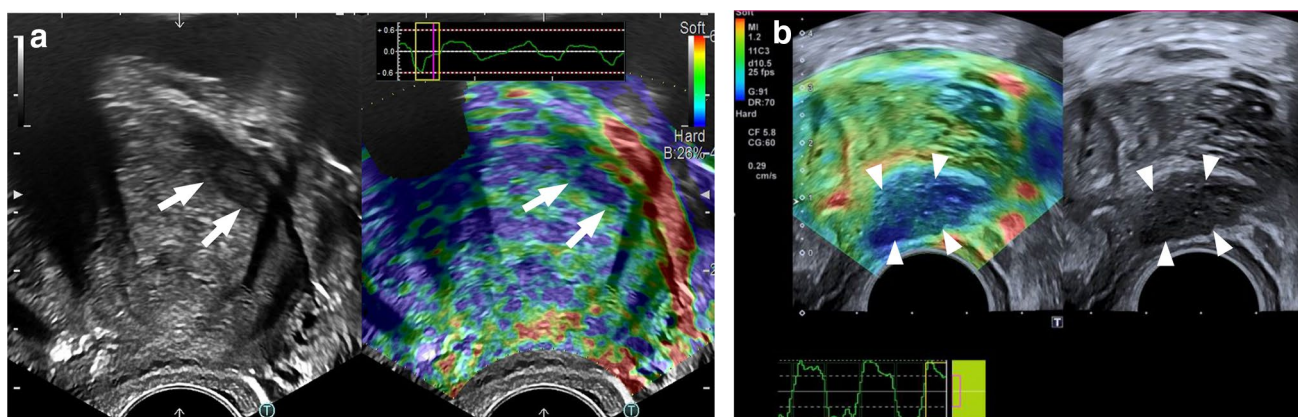


Fig. 5 Strain Elastography of a PCa. SE is performed using alternate compression and decompression cycles using the endocavitary transducer with the help of a quality curve. **a** 72-year-old patient with large prostate volume of 150 g, PSA 11 ng/mL, mp-MRI revealed a PIRADS 4 anterior lesion. The anterior subcapsular lesion (arrows) is very difficult to see on B-mode imaging (left side), and SE is helpful

to confirm that the hypoechoic anterior area is highly suspicious as it appears stiff on the elastogram (right side). TRUS-guided biopsy confirmed the presence of 12 mm/48 mm adenocarcinoma Gleason 3 + 3. **b** PCa Gleason 4 + 3 (arrow heads) was detected as a hypoechoic nodule (right side) with increased stiffness coded in blue on the elastogram (left side)

sensitivity and specificity of 60.8% and 68.4%, respectively [43]. PCa detection rates may be improved using SE-guided biopsy compared to B-mode guided biopsy (11.7–13.9%) [53, 54]. However, prostate SE is of limited value for small PCa detection and can miss low-grade lesions [43], such that SE cannot be used as a decision tool to rule out cancer without biopsy [43]. SE technical limitations include inadequate acquisitions due to prostate slippage in up to 32% of cases and low reproducibility, even in experienced hands [45, 55]. Detection rate is lower along the anterior parenchyma as compared to posterior areas, and also lower at prostate base compared to apical regions [44, 46, 47, 53]. In a recent study, SE was not superior to systematic biopsy in predicting subsequent PCa rates, and was, therefore, not considered an appropriate modality to determine which patients should undergo repeated prostate biopsy [56].

Shear-wave elastography (SWE)

In contrast to SE, it is mandatory to avoid any compression of the rectal wall with SWE. SWE is based on the measurement of shear wave velocity propagating transverse to the transmit ultrasound beam that induces an acoustic radiation force by quickly moving the focal point [57]. SWE provides a dynamic quantitative color map of soft tissues stiffness in quasi-real time. Mean elasticities are averaged

from a Quantitative box (Q-box) or ROI and displayed in kilo Pascal (kPa) or in m/sec as an overlay on the B-mode image. Stiff tissues are color coded in red, while soft tissues appear in blue, the opposite of the display pattern used for SE. Elasticity values (mean, standard deviation, min and max) are calculated for each ROI, and ratios between two Q-boxes placed in a suspicious region and in the adjacent normal peripheral zone can be calculated. This technology has only recently become available on end-fire endocavitary transducers, explaining the limited number of publications.

Prostate SWE must be conducted with optimized settings and an appropriate elasticity scale (70–90 kPa) in the transverse plane, waiting a few seconds at each imaging level for signal stabilization. The examination must be performed with minimal prostate compression, to minimize artifactual measurements. SWE may characterize a suspicious area or can be used for PCa detection, while scanning the prostate gland real time from base to apex. Depending on the prostate size, the SWE box can cover almost the entire gland (Fig. 6a), and digital cineloops may be saved for further review and post-scanning elasticity measurements. The elasticity values (mean, standard deviation, min and max) are then calculated for each ROI. Hypochoic lesions coded in red are suspicious for malignancy (Fig. 6b). In young patients without BPH, the peripheral and central zones are soft and color coded in blue with a homogeneous pattern

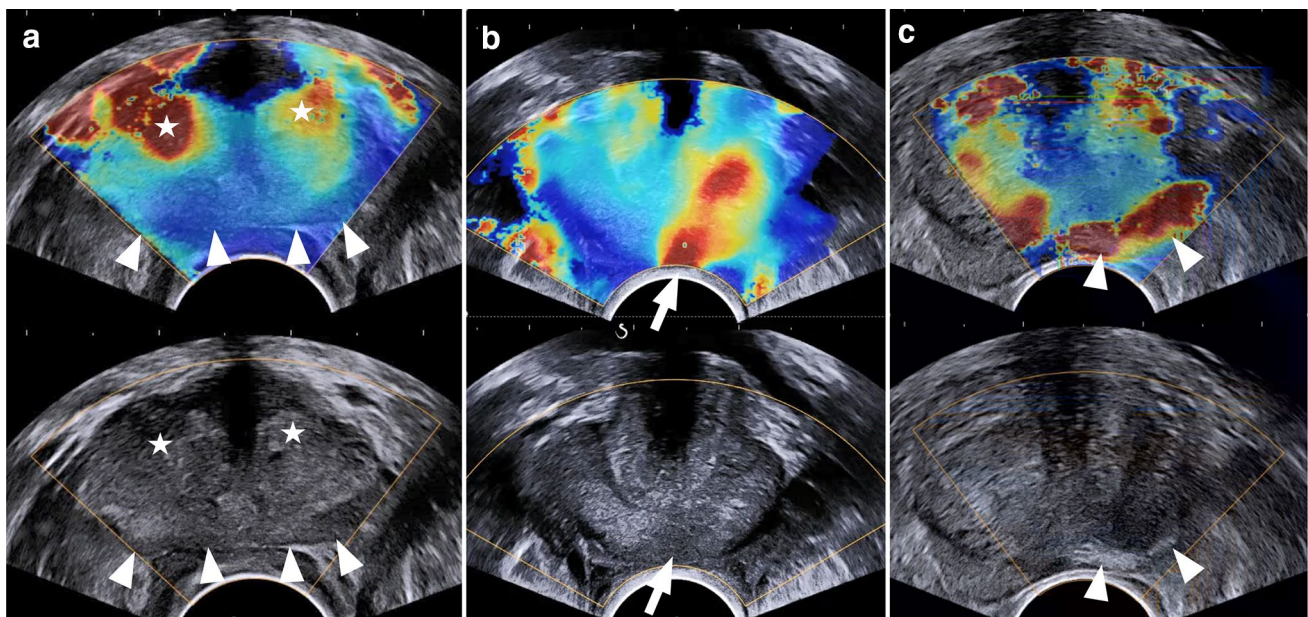


Fig. 6 Shear-Wave Elastography of normal tissue, PCa and calcified tissues. SWE elastograms are displayed real time at the top of the image with corresponding real-time B-mode plane at the bottom. **a** SWE at the prostate base in a 35-year-old patient with minimal BPH. The peripheral zone (arrow heads) is homogeneously soft and coded with blue colors, due to mean stiffness values typically below 30 kPa. The central zone exhibits some nodular areas (stars) with increased

stiffness below 70 kPa due to minimal development of BPH. The space in between the rectal wall and the posterior peripheral zone is coded in blue reflecting the minimal pressure induced by the endocavitary transducer. **b** Incidental discovery of a Gleason 7 (4+3) nodule with increased stiffness corresponding to a Gleason 4+3 PCa (arrow). **c** Typical artifact of increased stiffness due to the presence of macro-calcifications (arrow heads)

(with stiffness value ranging from 15 to 25 kPa); while, the transitional zone exhibit stiffness values below 70 kPa (Fig. 6a). With BPH development, the peripheral zone remains homogeneous and soft (blue colors); while, the transition zone becomes heterogeneous and stiff (red colors), with elasticity values ranging from 30 to 180 kPa [58].

In the hands of experienced sonographers, SWE exhibits excellent overall intra-observer reproducibility (ICC=0.876), with minimal impact of ROI location, prostate volume and clinical variables, presumably due to the lack of variability attributed to compression–decompression cycles with SE [59]. Real-time SWE sweeping through the prostate detects stiff nodules that are not visible at B-mode imaging. PCa usually appears stiffer as compared with surrounding tissue. Targeted biopsy can be performed under SWE guidance to increase the detection rate of cancer.

SWE applications include characterization of abnormal areas detected at TRUS (B-mode, CDUS or micro-Doppler imaging, but also at MRI), detection of stiff lesions not seen with other imaging techniques, and real-time targeting of biopsy cores. SWE diagnostic performances have been evaluated in a limited number of studies with almost all studies done on a single system (Aixplorer platform, SuperSonic Imagine, Aix-en-Provence, France). Accuracy, sensitivity, and negative predictive value (NPV) range from 70 to 96%, 92–96% (except for Woo et al. [59]), and 83–99% respectively [43]. In all studies, PCa stiffness was statistically significantly higher compared to benign lesions ($p < 0.002$). Although the clinical data are limited, there appears to be a correlation between SWE stiffness and Gleason score [60, 61]. The optimal threshold for PCa varies between studies, likely related to pre-compression effect, patient position (left lateral decubitus versus dorsal) and examination plane [58, 59, 62, 63]. A threshold of 35–37 kPa or a ratio between suspicious area and contralateral peripheral zone of 1.5 provided sensitivity, specificity, positive and NPV of 97%, 70%, 70%, and 97%, respectively, in a two-center study including 184 patients [61, 64]. These performances were similar to that of a recent study, despite the use of much higher cut-off values of 62.27 kPa, with sensitivity of 81.42% and specificity of 74.51% [65]. SWE increases PCa detection rate by 6.4-fold [66]. The addition of SWE increases the positive biopsy rate compared to that of TRUS [58, 61, 64, 66]. In the case of false-negative MRI, SWE can detect additional cs-PCa (2/3 of peripheral PCa missed by mp-MRI) [67]. However, SWE-targeted biopsies should always be performed in combination with systematic biopsies, and SWE is not sufficiently sensitive to exclude PCa without a biopsy [43]. Two recent meta-analyses of SWE for PCa detection found a pooled sensitivity of 83% (95% CI 0.66–0.92) and 86% (95% CI 0.75–0.92), and a pooled specificity of 85% (95% CI 0.78–0.90) and 89% (95% CI 0.82–0.93) [68, 69] and an overall high degree of accuracy with a summary receiver

operator characteristic curve with an AUC of 0.94 (95% CI 0.91–0.95) [69].

Prostate elastography limitations

Both SE and SWE face similar limitations, particularly in very large prostate glands. SE is unable to provide uniform compression of the entire gland. Shear waves are attenuated and cannot be extracted from the background noise in larger glands. Training is mandatory to limit intra- and inter-operator dependency, though training for SWE is shorter than for SE [43]. Additional SE limitations include slippage artifacts and the lack of quantitative information.

Pre-compression must be avoided when performing SWE, but this is difficult when there is a large prostate protruding toward the rectal wall. When excessive pressure is applied with SWE, the peripheral zone adjacent to the transducer appears stiff. Increased compression with the transducer will lead to higher cut-off values. SWE additional limitations include slow frame rate and delay in image stabilization.

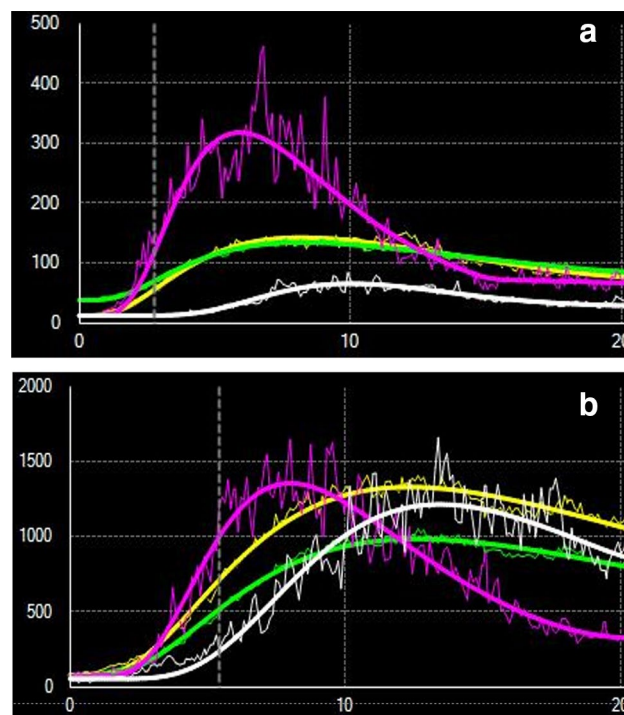


Fig. 7 Prostate CEUS and time–intensity curve (TIC) obtained from nodule (purple curve) and reference peripheral zone (yellow curve) in arbitrary units. SWE elastograms are displayed real time at the top of the image with corresponding real-time B-mode plane at the bottom. **a** The TIC is obtained from PCa. Note that the signal intensity is strongly higher than the reference parenchyma, but only lasts about 10 s. After the enhancement during the arterial phase, the nodule cannot be distinguished from the surrounding parenchyma. **b** The TIC is obtained from a nodule of prostatitis. Note that the signal intensity is similar than the reference parenchyma, but starts earlier

Artifacts in both SE and SWE techniques occur in the presence of macro-calcifications (Fig. 6c). Interpretation must combine the analysis of both B-mode image and elasticity maps acquired at the same plane. Both SE and SWE suffer from the same intrinsic limitations as all cancers are not stiff and all stiff lesions are not cancers.

Contrast-enhanced ultrasound (CEUS)

In a very similar approach to that of CT and MRI, ultrasound contrast agents (UCAs) are available for intravenous administration to enhance Doppler and gray-scale vascular signals. CEUS can be used off-label for prostate disease assessment [70]. The active ingredient of all approved UCAs is microbubbles and their tolerance in clinical practice is excellent with the incidence of serious anaphylactoid reactions well below that of iodinated contrast media ($\approx 0.014\%$) [70]. Microbubbles are blood pool agents and do not reach the interstitial space or the urine. UCAs do not have renal toxicity and are not contra-indicated in case of renal insufficiency or obstruction. A prostate CEUS examination is performed using the transrectal transducer at low acoustic power (mechanical index below 0.2) with dedicated contrast imaging sequences that allow detection of the nonlinear microbubble ultrasonic response. PCa exhibits earlier and

increased enhancement compared to surrounding benign parenchyma (Fig. 7). Furthermore, newer CEUS techniques allow visualization of microvascular anatomy; vessels that supply areas of tumor are more numerous and irregular in configuration as compared with the normal radially oriented vessels that extend into the prostate parenchyma from the neurovascular bundles and periurethral vascular plexus (Fig. 4).

CEUS challenges

Prostate CEUS faces several challenges related to microbubble properties, to prostate gland anatomy and to PCa perfusion. Indeed, the resonant frequency of most UCAs is close to 2 MHz, while TRUS transducer frequency ranges from 3 to 12 MHz: thus, only a limited number of the smaller size microbubbles administered intravenously provide the harmonic signals from resonating microbubbles. Furthermore, prostate perfusion is limited when compared to the kidneys or liver. PCa enhancement is transient during arterial phase and can be distinguished from the surrounding parenchyma for less than 20 s after UCA bolus injection. Although these technical limitations are correct in principle, excellent enhancement of the prostate is nowadays obtained with standard clinical doses of UCAs. A more important limitation is the development of BPH which increases the size

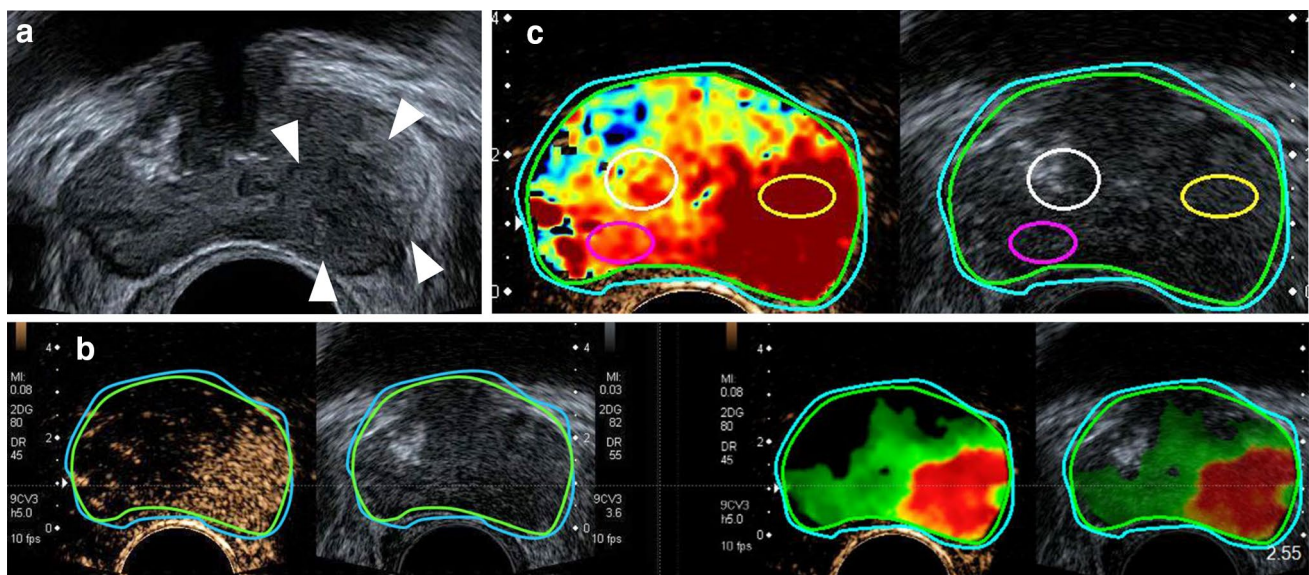


Fig. 8 PCa CEUS parametric imaging and dispersion imaging. **a** Non-linear B-mode imaging identified a heterogeneous nodule with poorly defined borders (arrow heads). **b** CEUS prostate cineloop processed with research software derived from VueBox® (Bracco SA, Geneva, Switzerland). In the left sided image pair, prostate CEUS is displayed, demonstrating a real-time low-mechanical index harmonic contrast image on left side of the pair, and a reference low-mechanical index B-mode reference on the right side of this pair. PCa

demonstrates intense enhancement in the left peripheral zone, extending to the transition zone. In the right sided image pair, a dispersion image is calculated based upon the wash-in rate histogram; this technique identifies PCa without placing an ROI, thus, avoiding operator dependency related to ROI location and size. **c** Further quantification can be performed by placing ROIs upon the suspected PCa as well as upon normal contralateral peripheral and transition zones

and vascularity of the transition zone, and may overshadow the flow associated with malignancy. Finally, PCa enhancement is transient during the intravascular phase, limiting the usable vascular enhancement to under one minute after a bolus injection of UCA (Fig. 7). As prostate adenocarcinoma does not exhibit reliable wash-out, the short wash-in phase is more useful. Furthermore, in many published studies, prostate CEUS starts with identification of the most suspicious area, whatever the technique (B-mode, color or micro-Doppler imaging, elastography, or even MRI with cognitive or software-assisted registration). The transducer is maintained at this level and a bolus injection of UCA is performed (for SonoVue® 2.4 ml) after switching imaging mode to low acoustic power contrast imaging. With this single-level technique, one can question the role of prostate CEUS since the reference diagnostic method has already identified the site for targeted biopsy. The duration of PCa enhancement after bolus injection of the UCA can be extended by infusion of the UCA. The stability of the diluted microbubbles may vary depending on the UCA. Prostate CEUS using UCA infusion may allow PCa detection by evaluation of the microvascular anatomy with a continuous imaging sweep through the prostate during the steady-state intravascular phase. The steady-state intravascular phase of UCAs can be used to evaluate vascular density and microvessel morphology [71].

CEUS diagnostic performance

Preliminary studies focused on PCa detection using power Doppler imaging and Levovist®, the first transpulmonary UCA approved in Europe for radiology indications. CEUS improved the detection of the hypervascularity of PCa nodules, increasing both sensitivity from 54 to 93%, and specificity from 79 to 87% for baseline Doppler examination and CEUS examination, respectively [72]. PCa detection rate was significantly better for contrast-enhanced color-Doppler-targeted biopsies than for systematic biopsy in the largest clinical trial involving 1776 patients, 10.8% vs. 5.1%, respectively [73]. However, conventional Doppler imaging is not the most appropriate technique to visualize the effect of UCA due to the huge signal enhancement resulting in blooming artifacts. Real-time low acoustic power imaging harmonic gray-scale imaging is most suitable for prostate CEUS. Using gray-scale harmonic imaging, CEUS demonstrates improved diagnostic accuracy for PCa diagnosis compared to pre-contrast imaging, particularly for high-grade cancer (GS ≥ 7) with more than 50% biopsy core involvement, compared to pre-contrast imaging ($p = 0.001$) in a large prospective study of 272 patients (ROC area under the curve 0.90) [74]. In a large prospective study enrolling 1024 patients, CEUS-targeted biopsies detected 67/326 (20.5%) additional cases of cs-PCa, including 51 patients (15.6%) missed by systematic biopsy [75]. The single meta-analysis

of prostate CEUS performance included 16 papers and 2624 patients. Despite statistically significant between-study heterogeneity ($p < 0.001$), CEUS appears as a promising tool for PCa detection with pooled sensitivity, pooled specificity and odds ratio of 70%, 74% and 9.09, respectively. Nonetheless, CEUS is not adequately sensitive to avoid systematic biopsy [76]. In addition to PCa detection, CEUS can provide

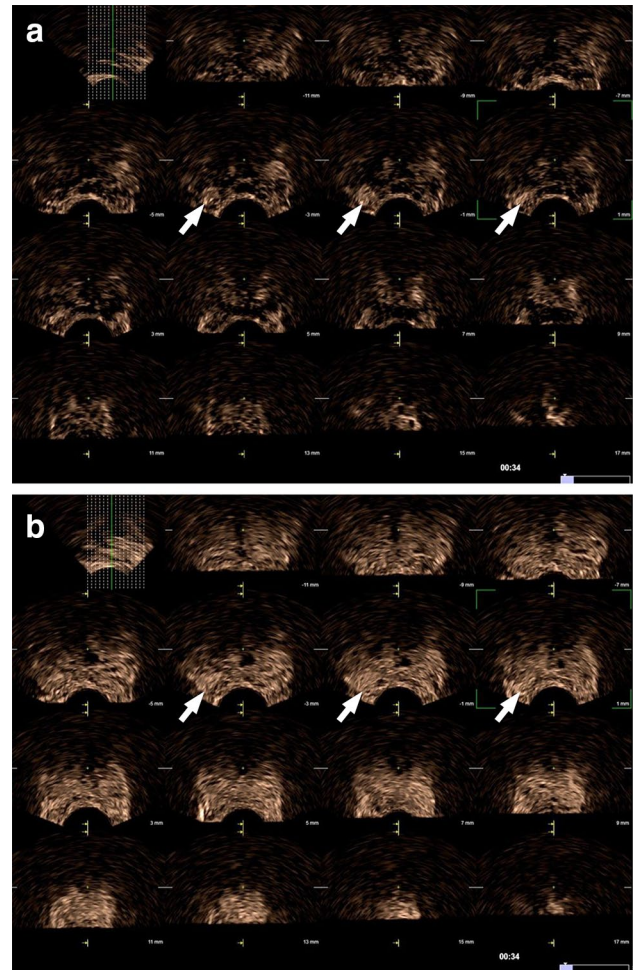


Fig. 9 4D-CEUS in a patient with a suspicious nodule on mid-left peripheral zone. TRUS 4D-CEUS was performed following a bolus injection of 2.4 mL of Sonovue (BR1, Bracco SA, Mila, Italy) using an end-fire mechanical transducer (9CV3, Toshiba MS, Nasu, Japan). 3D volumes are acquired at 1.4 volumes per sec (one volume acquired each 0.7 s), during wash-in and wash-out phases. MPR are reconstructed with a 2-mm slice thickness from base to apex. The major advantage of this approach is the potential to detect early and strong enhancement of the entire prostate at high volume rate. **a** Early volume acquisition during arterial phase. No abnormal enhancement is detected at the level of the suspicious area on the left side. However, a nodule is detected at mid part of the right gland inside the lateral peripheral zone (arrows). **b** Five seconds later, the normal gland has enhanced and the contrast resolution between the nodule and the normal parenchyma resolved; the nodule is not visible anymore (arrows). This transient but significant enhancement requires high volume rate and complete assessment of prostate volume

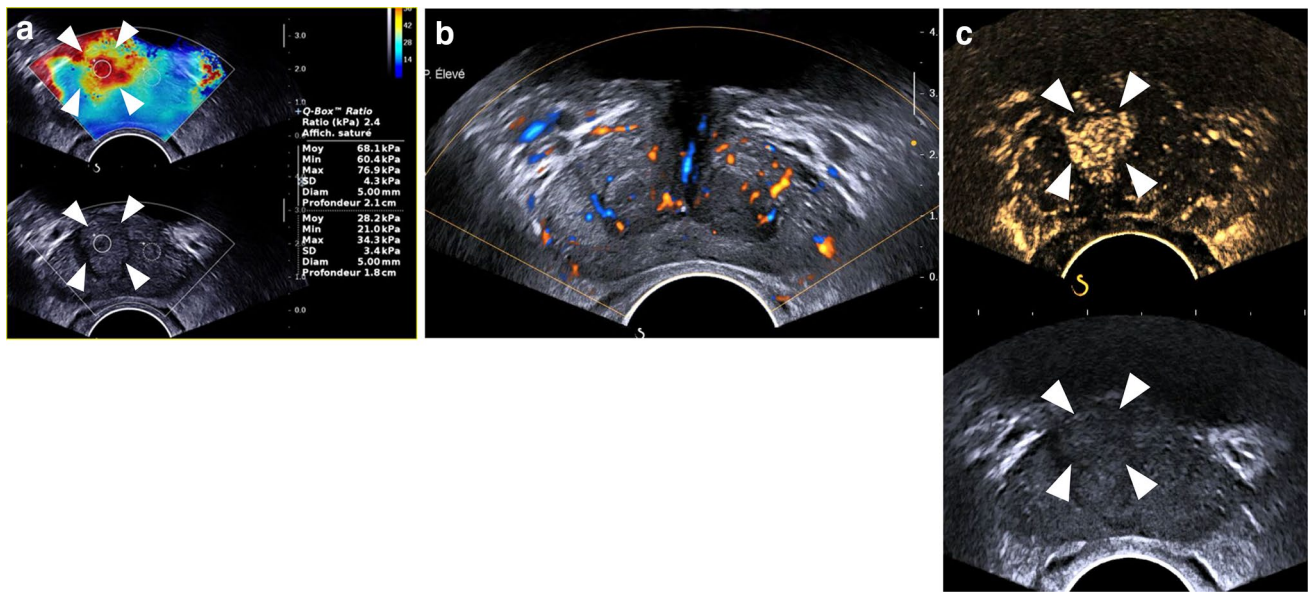


Fig. 10 Diagnosis of PCa using mp-US—case 1. Seventy-two-year-old man with moderate increase of PSA at 6.3 ng/mL, remaining stable for the past year (no previous data). MRI cannot be performed due to non-compatible PaceMaker. A previous US study did not show any suspicious area. Mp-US started with conventional and enhanced B-mode imaging, and was followed with conventional and micro-Doppler imaging. It did not show any abnormal nodule. **a** SWE scan started at prostate base and immediately revealed a nodule with increased stiffness in anterior central zone (arrows). SWE allowed

quantitative measurements of stiffness, in this case mean nodule stiffness is 68 kPa, while contralateral central zone mean stiffness was 28 kPa. **b** Color-Doppler US at the same level did not reveal any B-mode or blood flow disturbance. **c** CEUS confirmed the presence of a hypervascular nodule. Three biopsies targeting this suspicious area confirmed the presence of an adenocarcinoma Gleason 8 (22 mm of PCa); while all systematic biopsies showed no PCa. Radical prostatectomy confirmed the presence of a single cs-PCa at the same location

assessment of hypoperfusion and necrosis after focal therapy with high-intensity focused ultrasound for low-grade cancer, or prostate artery embolization for BPH [77, 78].

Two different approaches have been tested to overcome prostate CEUS limitations: perfusion quantification with parametric imaging and 4D trans-rectal CEUS imaging. The change in signal intensity calculated from a ROI after intravenous injection of the UCA can be plotted over time and is called time–intensity curve (TIC) (Fig. 7). Typically, a ROI is located upon an abnormal area and another reference ROI is positioned on normal enhancing parenchyma (contralateral parenchyma). Significant PCa (ISUP ≥ 2 , i.e., Gleason score ≥ 7) exhibits higher peak enhancement, shorter rise time and shorter time to peak [79]. However, this approach assumes that the area of abnormality is detected by the operator. To improve the detection of abnormal enhancement, it is possible to compute a TIC over the entire image and automatically estimate the heterogeneity of the enhancement based on the dispersion on the histogram of the wash-in rate [80, 81]. The software can automatically draw areas with abnormal enhancement (Fig. 8). Parametric dispersion CEUS had better performance (with 91% sensitivity, 56% specificity, 57% positive predictive value (PPV) and 90% NPV) than CEUS alone (with 73% sensitivity, 58%

specificity, 50% PPV and 79% NPV) [82]. These areas can be further targeted with biopsy. 4D TR-CEUS is another approach to overcome the limited duration of PCa enhancement compared to the surrounding parenchyma. The end-fire transducer can be mechanically driven through the prostate to acquire prostate volumes using contrast harmonic imaging after injection of the UCA. Volumes can be reconstructed and multiplanar reconstructions (MPR) performed (Fig. 9). The volume rate can be increased up to 1.5 vps, so that 5–10 volumes can be obtained before saturation of the prostate with microbubbles that wipes out contrast resolution between PCa and normal parenchyma. MPR can be displayed to identify areas of earlier and stronger enhancement (Fig. 9), and targeted biopsies can be planned.

CEUS provides a large amount of quantitative data that may enhance the diagnosis of PCa by the use of properly trained machine-learning algorithms to go beyond simple analysis of kinetics models [83]. Such an approach using support vector machines has been tested for CEUS liver tumor characterization with excellent performances (94% sensitivity, 87.1% specificity and 91.8% accuracy) [84]. Preliminary studies suggest that the combination of perfusion and dispersion CEUS parameters using a Gaussian mixture model can improve PCa localization as well [85].

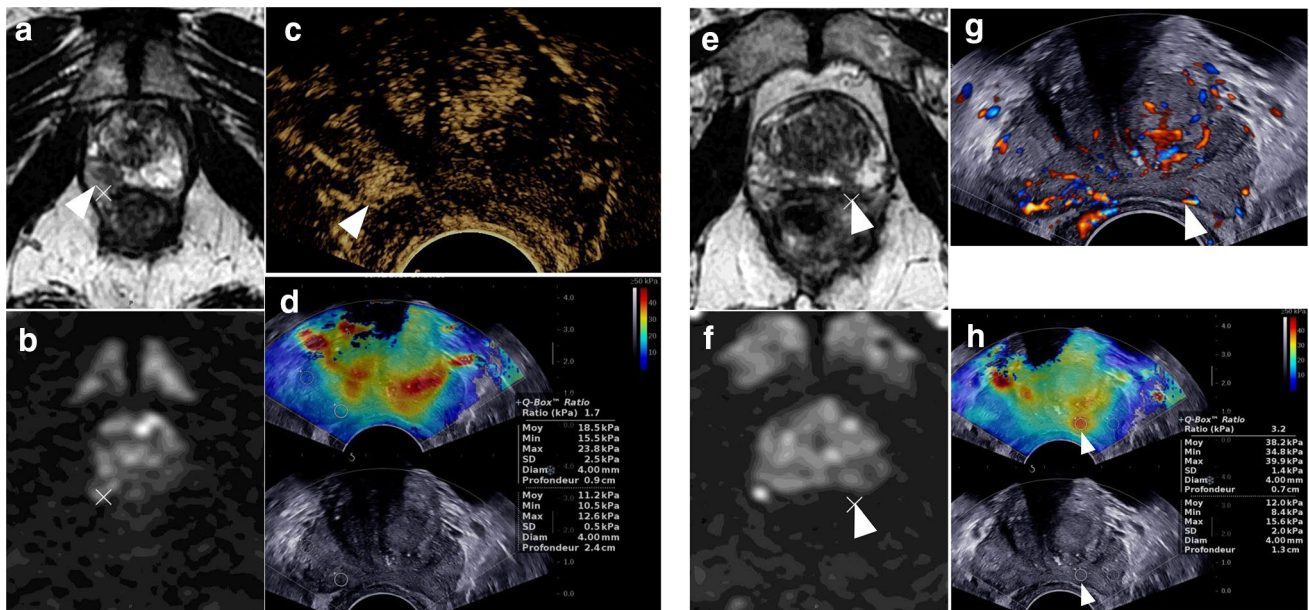


Fig. 11 Diagnosis of PCa using mp-US—case 2. Seventy-one-year-old man with growing PSA (4.2 ng/mL in 2017, 5.6 ng/mL in 2019 and 9.5 ng/mL in January 2020) and prostate volume of 50 g. In September 2019, the MRI study revealed 2 peripheral zone nodules PIRADS 2 (right side, 9 mm) and PIRADS 3 (left side 8 mm). Systematic biopsies performed by the urologist revealed on both sides sub millimeter adenocarcinoma Gleason 6 (3+3) for two cores on right side and one core on left side (sum of cancer length from all cores: 2.4 mm). Recommended treatment was active surveillance. The patient was referred for re-evaluation: a new MRI study performed in January 2020 confirmed the lack of PIRADS 4 or 5 lesion and maintained the two small nodules as PIRADS 2 (right) and 3 (left) lesions. **a, b** MRI study of the right nodule with T2-weighted sequence (**a**, arrow) and diffusion-weighted sequence (**b**). The lesion was not seen on ADC map and did not enhance differently than surrounding tissue (not shown). **c** At CEUS, the nodule exhibited early and intense enhancement (arrow head). **d** The nodule stiffness was slightly increased but remained below the threshold of 35 kPa. Pros-

tate biopsy (3 cores) revealed the presence of a mucinous well-differentiated carcinoma Gleason 3+3 (2-mm PCa of 36-mm tissue sample). **e, f** MRI study of the left nodule with T2-weighted sequence (**e**, arrow) and diffusion-weighted sequence (**f**). The lesion was not seen on ADC map and did not enhance differently than surrounding tissue (not shown). **g** At CDUS, the nodule vascularity is not increased and it is poorly seen at underlying B-mode imaging (arrow head). **h** The nodule stiffness was significantly increased at SWE (mean stiffness value 38 kPa) with a ratio of 3.2 compared to the adjacent normal peripheral zone. These values are typical for PCa. Prostate biopsy (3 cores) revealed the presence of a mucinous well-differentiated carcinoma Gleason 3+4 (11-mm PCa of 28-mm tissue sample; 45% of Gleason 4). The systematic biopsy of the same sextant also showed adenocarcinoma Gleason 3+4 (5-mm PCa of 12-mm tissue sample; BUT with only 30% of Gleason 4). Recommended treatment changed to invasive treatment (radical prostatectomy or radiotherapy). Patient and tumor board decision was radical prostatectomy

What is multiparametric ultrasound?

The concept of multiparametric ultrasound (mp-US) derives from mp-MRI. Advanced prostate US takes advantage of the benefits of improved B-mode US, vascular imaging techniques, US elastography and perfusion imaging, with next-generation examination performed using volumetric imaging (3D and 4D imaging) [86]. Mp-US performance may be similar to that of mp-MRI (mp-US: 0.874 ± 0.043 , 95% confidence interval, 0.790–0.959, compared to mp-MRI: 0.774 ± 0.055 , 95% confidence interval, 0.666–0.881 [87].

In practice, today's workflow for patients referred for prostate biopsy often starts with a careful reading of a mp-MRI for identification of targets [88]. Mp-US begins with TRUS transverse and sagittal acquisitions using improved B-mode and conventional color/power Doppler imaging using optimized settings. Additional techniques, including

micro-Doppler elastography and CEUS are performed for detection of additional targets. If no lesion is detected, systematic biopsies are performed using various protocols, depending on patient status (biopsy naïve, active surveillance, follow-up after treatment, etc). In the presence of a suspicious area, single-level CEUS following a bolus of UCA may be complementary to other techniques to confirm the presence or the location of the suspicious lesion (Figs. 10, 11). Finally, a map including mp-MRI and mp-US targets is prepared for optimal biopsy planning, including lesion stratification score (lesions being at higher risk of PCa). MRI-US fusion is helpful particularly when the target is only detected at MRI. Fusion can be performed with all US modalities, including B-mode, color-Doppler, micro-Doppler, SWE and CEUS (Fig. 12).

Future mp-US targeting will incorporate newer developments in Artificial Intelligence and machine learning [83].

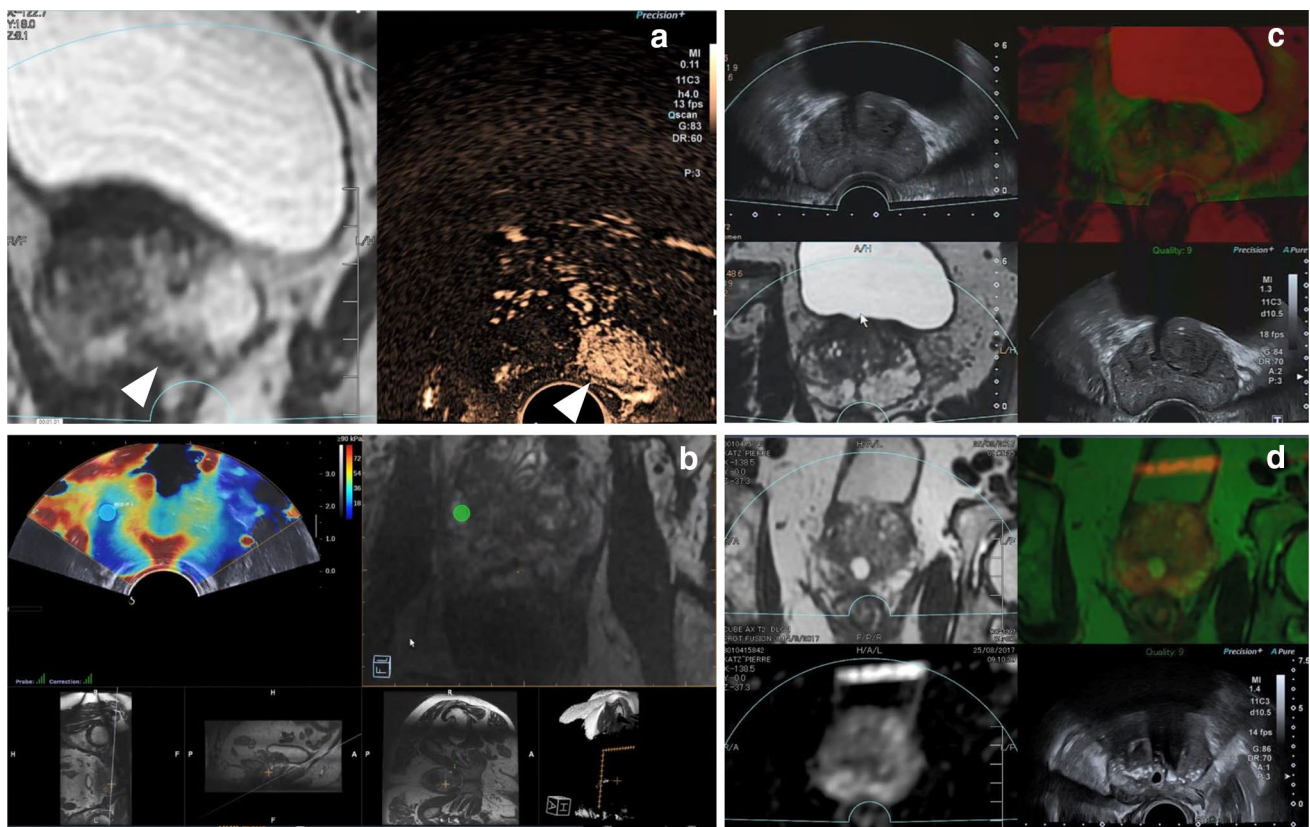


Fig. 12 mp-MRI-mp-US fusion imaging. Mp-US can be fused with mp-MRI to improved targeted biopsy. **a** Fusion imaging between MRI T2-weighted sequence and CEUS (arrow head indicating PCa). **b** Fusion imaging between MRI T2-weighted sequence and SWE. **c**

Automatic fusion procedure between MRI T2-weighted sequence and Conventional B-mode imaging. **d** Fusion procedure between MRI T2- and diffusion-weighted sequences and Conventional B-mode imaging

Mp-US using B-mode, SWE and CEUS radiomics will improve PCa localization using machine learning, outperforming the best-performing single parameter [89]. The development of more powerful deep-learning algorithms will allow the combination of functional and molecular parameters. These developments should also include MRI data.

Advanced prostate US imaging techniques have incremental improvements in detection of PCa, but up to now, none are providing sufficient accuracy when considered separately. Their combination, especially with elastography and CEUS, is more powerful but the overall evaluation of patients with a suspicion of PCa cannot obviate the utility of mp-MRI and the potential of fusion information. Indeed, these two non-invasive imaging techniques—mp-US using advanced techniques and mp-MRI—provide complementary information which will become even more important in the era of focal therapy, where precise identification of PCa location is needed.

Author contributions JMC: Project development, Data collection, Manuscript writing. EH: Project development, Manuscript writing. RB: Project development, Manuscript writing. GS: Manuscript writing. JW: Manuscript writing. SB: Data collection, Manuscript writing. CD: Data collection, Manuscript writing. JR: Project development, Manuscript writing.

Compliance with ethical standards

Conflict of interest JM Correas: Speakers fees: Canon MS, General Electric MS, Hitachi MS, Philips Ultrasound, Siemens Ultrasound, Supersonic Imagine. Equipment grants: Canon MS, Hitachi MS, Philips Ultrasound, SuperSonic Imagine. E Halpern: No potential conflict of interest. R Barr: Project development, Manuscript writing. Speakers fees: Philips Ultrasound, Siemens Ultrasound, Mindray, Canon. Equipment grants: Philips Ultrasound, Siemens Ultrasound, Mindray Ultrasound, SuperSonic Imagine, Canon Ultrasound, Samsung Ultrasound, GE Medical Royalties: Thieme Publishers Advisory panel-Samsung Ultrasound. G Sangeet: No potential conflict of interest. J Walz: No potential conflict of interest. S Bodard: No potential conflict of interest. C Dariane: No potential conflict of interest. J de la Rosette: No potential conflict of interest.

References

- Mottet N, Bellmunt J, Bolla M et al (2017) EAU-ESTRO-SIOG guidelines on prostate cancer. Part 1: screening, diagnosis, and local treatment with curative intent. *Eur Urol* 71:618–629. <https://doi.org/10.1016/j.eururo.2016.08.003>
- Hayes JH, Barry MJ (2014) Screening for prostate cancer with the prostate-specific antigen test: a review of current evidence. *JAMA* 311:1143–1149. <https://doi.org/10.1001/jama.2014.2085>
- Olleik G, Kassouf W, Aprikian A et al (2018) Evaluation of new tests and interventions for prostate cancer management: a systematic review. *J Natl Compr Cancer Netw JNCCN* 16:1340–1351. <https://doi.org/10.6004/jnccn.2018.7055>
- Kelloff GJ, Choyke P, Coffey DS, Prostate Cancer Imaging Working Group (2009) Challenges in clinical prostate cancer: role of imaging. *AJR Am J Roentgenol* 192:1455–1470. <https://doi.org/10.2214/AJR.09.2579>
- Mian BM, Naya Y, Okihara K et al (2002) Predictors of cancer in repeat extended multisite prostate biopsy in men with previous negative extended multisite biopsy. *Urology* 60:836–840. [https://doi.org/10.1016/S0090-4295\(02\)01950-7](https://doi.org/10.1016/S0090-4295(02)01950-7)
- Singh H, Canto EI, Shariat SF et al (2004) Predictors of prostate cancer after initial negative systematic 12 core biopsy. *J Urol* 171:1850–1854. <https://doi.org/10.1097/01.ju.0000119667.86071.e7>
- Delongchamps NB, Haas GP (2009) Saturation biopsies for prostate cancer: current uses and future prospects. *Nat Rev Urol* 6:645–652. <https://doi.org/10.1038/nrurol.2009.213>
- Giannarini G, Autorino R, di Lorenzo G (2009) Saturation biopsy of the prostate: why saturation does not saturate. *Eur Urol* 56:619–621. <https://doi.org/10.1016/j.eururo.2009.03.044>
- Ashley RA, Inman BA, Routh JC et al (2008) Reassessing the diagnostic yield of saturation biopsy of the prostate. *Eur Urol* 53:976–981. <https://doi.org/10.1016/j.eururo.2007.10.049>
- Nougaret S, Robertson N, Golia Pernicka J et al (2017) The performance of PI-RADSv2 and quantitative apparent diffusion coefficient for predicting confirmatory prostate biopsy findings in patients considered for active surveillance of prostate cancer. *Abdom Radiol NY* 42:1968–1974. <https://doi.org/10.1007/s00261-017-1086-7>
- Bloom JB, Hale GR, Gold SA et al (2019) Predicting Gleason Group progression for men on prostate cancer active surveillance: role of a negative confirmatory magnetic resonance imaging-ultrasound fusion biopsy. *J Urol* 201:84–90. <https://doi.org/10.1016/j.juro.2018.07.051>
- Richenberg J, Løgager V, Panebianco V et al (2019) The primacy of multiparametric MRI in men with suspected prostate cancer. *Eur Radiol* 29:6940–6952. <https://doi.org/10.1007/s00330-019-06166-z>
- Faria R, Soares MO, Spackman E et al (2018) Optimising the diagnosis of prostate cancer in the era of multiparametric magnetic resonance imaging: a cost-effectiveness analysis based on the Prostate MR Imaging Study (PROMIS). *Eur Urol* 73:23–30. <https://doi.org/10.1016/j.eururo.2017.08.018>
- Rouvière O, Puech P, Renard-Penna R et al (2019) Use of prostate systematic and targeted biopsy on the basis of multiparametric MRI in biopsy-naïve patients (MRI-FIRST): a prospective, multicentre, paired diagnostic study. *Lancet Oncol* 20:100–109. [https://doi.org/10.1016/S1470-2045\(18\)30569-2](https://doi.org/10.1016/S1470-2045(18)30569-2)
- Vargas HA, Akin O, Shukla-Dave A et al (2012) Performance characteristics of MR imaging in the evaluation of clinically low-risk prostate cancer: a prospective study. *Radiology* 265:478–487. <https://doi.org/10.1148/radiol.12120041>
- Fütterer JJ, Briganti A, De Visschere P et al (2015) Can clinically significant prostate cancer be detected with multiparametric magnetic resonance imaging? A systematic review of the literature. *Eur Urol* 68:1045–1053. <https://doi.org/10.1016/j.eururo.2015.01.013>
- Johnson DC, Raman SS, Mirak SA et al (2019) Detection of individual prostate cancer foci via multiparametric magnetic resonance imaging. *Eur Urol* 75:712–720. <https://doi.org/10.1016/j.eururo.2018.11.031>
- Niaf É, Flamary R, Rouvière O et al (2014) Kernel-based learning from both qualitative and quantitative labels: application to prostate cancer diagnosis based on multiparametric MR imaging. *IEEE Trans Image Process Publ IEEE Signal Process Soc* 23:979–991. <https://doi.org/10.1109/TIP.2013.2295759>
- Dinh AH, Melodelima C, Souchon R et al (2018) Characterization of prostate cancer with gleason score of at least 7 by using quantitative multiparametric mr imaging: validation of a computer-aided diagnosis system in patients referred for prostate biopsy. *Radiology* 287:525–533. <https://doi.org/10.1148/radiol.2017171265>
- Norberg M, Egevad L, Holmberg L et al (1997) The sextant protocol for ultrasound-guided core biopsies of the prostate underestimates the presence of cancer. *Urology* 50:562–566. [https://doi.org/10.1016/S0090-4295\(97\)00306-3](https://doi.org/10.1016/S0090-4295(97)00306-3)
- Beerlage HP, Aarnink RG, Ruijter ET et al (2001) Correlation of transrectal ultrasound, computer analysis of transrectal ultrasound and histopathology of radical prostatectomy specimen. *Prostate Cancer Prostatic Dis* 4:56–62. <https://doi.org/10.1038/sj.pcan.4500495>
- Cheng S, Rifkin MD (2001) Color Doppler imaging of the prostate: important adjunct to endorectal ultrasound of the prostate in the diagnosis of prostate cancer. *Ultrasound Q* 17:185–189. <https://doi.org/10.1097/00013644-200109000-00008>
- Zhai L, Madden J, Foo W-C et al (2010) Characterizing stiffness of human prostates using acoustic radiation force. *Ultrason Imaging* 32:201–213. <https://doi.org/10.1177/01617346103200401>
- Baumgart LA, Gerling GJ, Bass EJ (2010) Characterizing the range of simulated prostate abnormalities palpable by digital rectal examination. *Cancer Epidemiol* 34:79–84. <https://doi.org/10.1016/j.canep.2009.12.002>
- Smith DS, Catalona WJ (1995) Interexaminer variability of digital rectal examination in detecting prostate cancer. *Urology* 45:70–74. [https://doi.org/10.1016/S0090-4295\(95\)96812-1](https://doi.org/10.1016/S0090-4295(95)96812-1)
- Lughezzani G, Saita A, Lazzeri M et al (2019) Comparison of the diagnostic accuracy of micro-ultrasound and magnetic resonance imaging/ultrasound fusion targeted biopsies for the diagnosis of clinically significant prostate cancer. *Eur Urol Oncol* 2:329–332. <https://doi.org/10.1016/j.euo.2018.10.001>
- Loch T (2007) Computerized transrectal ultrasound (C-TRUS) of the prostate: detection of cancer in patients with multiple negative systematic random biopsies. *World J Urol* 25:375–380. <https://doi.org/10.1007/s00345-007-0181-8>
- Strunk T, Decker G, Willinek W et al (2014) Combination of C-TRUS with multiparametric MRI: potential for improving detection of prostate cancer. *World J Urol* 32:335–339. <https://doi.org/10.1007/s00345-012-0924-z>
- Braeckman J, Autier P, Soviany C et al (2008) The accuracy of transrectal ultrasonography supplemented with computer-aided ultrasonography for detecting small prostate cancers. *BJU Int* 102:1560–1565. <https://doi.org/10.1111/j.1464-410X.2008.07878.x>
- Sivaraman A, Sanchez-Salas R, Barret E et al (2015) Prostate histoscanning true targeting guided prostate biopsy: initial clinical experience. *World J Urol* 33:1475–1479. <https://doi.org/10.1007/s00345-014-1434-y>
- Schiffmann J, Mehring G, Tennstedt P et al (2016) True targeting-derived prostate biopsy: HistoScanning™ remained inadequate

- despite advanced technical efforts. *World J Urol* 34:495–500. <https://doi.org/10.1007/s00345-015-1637-x>
32. Wysock JS, Xu A, Orczyk C, Taneja SS (2017) Histo scanning TM to detect and characterize prostate cancer—a review of existing literature. *Curr Urol Rep* 18:97. <https://doi.org/10.1007/s11934-017-0747-y>
 33. Wildeboer RR, van Sloun RJG, Wijkstra H, Mischi M (2020) Artificial intelligence in multiparametric prostate cancer imaging with focus on deep-learning methods. *Comput Methods Progr Biomed* 189:105316. <https://doi.org/10.1016/j.cmpb.2020.105316>
 34. Dvorak HF (1986) Tumors: wounds that do not heal. Similarities between tumor stroma generation and wound healing. *N Engl J Med* 315:1650–1659. <https://doi.org/10.1056/NEJM198612253152606>
 35. Tuxhorn JA, Ayala GE, Rowley DR (2001) Reactive stroma in prostate cancer progression. *J Urol* 166:2472–2483
 36. Barron DA, Rowley DR (2012) The reactive stroma microenvironment and prostate cancer progression. *Endocr Relat Cancer* 19:R187–204. <https://doi.org/10.1530/ERC-12-0085>
 37. Tuxhorn JA, Ayala GE, Smith MJ et al (2002) Reactive stroma in human prostate cancer: induction of myofibroblast phenotype and extracellular matrix remodeling. *Clin Cancer Res* 8:2912–2923
 38. Phipps S, Yang THJ, Habib FK et al (2005) Measurement of tissue mechanical characteristics to distinguish between benign and malignant prostatic disease. *Urology* 66:447–450. <https://doi.org/10.1016/j.urology.2005.03.017>
 39. Hoyt K, Castaneda B, Zhang M et al (2008) Tissue elasticity properties as biomarkers for prostate cancer. *Cancer Biomark Sect Dis Markers* 4:213–225. <https://doi.org/10.3233/cbm-2008-44-505>
 40. Zhang M, Nigwekar P, Castaneda B et al (2008) Quantitative characterization of viscoelastic properties of human prostate correlated with histology. *Ultrasound Med Biol* 34:1033–1042. <https://doi.org/10.1016/j.ultrasmedbio.2007.11.024>
 41. Ahn B-M, Kim J, Ian L et al (2010) Mechanical property characterization of prostate cancer using a minimally motorized indenter in an ex vivo indentation experiment. *Urology* 76:1007–1011. <https://doi.org/10.1016/j.urology.2010.02.025>
 42. Carson WC, Gerling GJ, Krupski TL et al (2011) Material characterization of ex vivo prostate tissue via spherical indentation in the clinic. *Med Eng Phys* 33:302–309. <https://doi.org/10.1016/j.medengphy.2010.10.013>
 43. Barr RG, Cosgrove D, Brock M et al (2017) WFUMB guidelines and recommendations on the clinical use of ultrasound elastography: part 5. *Prostate Ultrasound Med Biol* 43:27–48. <https://doi.org/10.1016/j.ultrasmedbio.2016.06.020>
 44. Tsutsumi M, Miyagawa T, Matsumura T et al (2010) Real-time balloon inflation elastography for prostate cancer detection and initial evaluation of clinicopathologic analysis. *AJR Am J Roentgenol* 194:W471–476. <https://doi.org/10.2214/AJR.09.3301>
 45. Miyagawa T, Tsutsumi M, Matsumura T et al (2009) Real-time elastography for the diagnosis of prostate cancer: evaluation of elastographic moving images. *Jpn J Clin Oncol* 39:394–398. <https://doi.org/10.1093/jjco/hyp026>
 46. Junker D, Schäfer G, Aigner F et al (2012) Potentials and limitations of real-time elastography for prostate cancer detection: a whole-mount step section analysis. *Sci World J* 2012:193213. <https://doi.org/10.1100/2012/193213>
 47. Junker D, Schäfer G, Kobel C et al (2014) Comparison of real-time elastography and multiparametric MRI for prostate cancer detection: a whole-mount step-section analysis. *AJR Am J Roentgenol* 202:W263–269. <https://doi.org/10.2214/AJR.13.11061>
 48. Sumura M, Shigeno K, Hyuga T et al (2007) Initial evaluation of prostate cancer with real-time elastography based on step-section pathologic analysis after radical prostatectomy: a preliminary study. *Int J Urol Off J Jpn Urol Assoc* 14:811–816. <https://doi.org/10.1111/j.1442-2042.2007.01829.x>
 49. Zhu Y, Chen Y, Qi T et al (2014) Prostate cancer detection with real-time elastography using a bi-plane transducer: comparison with step section radical prostatectomy pathology. *World J Urol* 32:329–333. <https://doi.org/10.1007/s00345-012-0922-1>
 50. Zhang B, Ma X, Zhan W et al (2014) Real-time elastography in the diagnosis of patients suspected of having prostate cancer: a meta-analysis. *Ultrasound Med Biol* 40:1400–1407. <https://doi.org/10.1016/j.ultrasmedbio.2014.02.020>
 51. Pallwein L, Mitterberger M, Struve P et al (2007) Comparison of sonoelastography guided biopsy with systematic biopsy: impact on prostate cancer detection. *Eur Radiol* 17:2278–2285. <https://doi.org/10.1007/s00330-007-0606-1>
 52. Aigner F, Pallwein L, Junker D et al (2010) Value of real-time elastography targeted biopsy for prostate cancer detection in men with prostate specific antigen 1.25 ng/ml or greater and 4.00 ng/ml or less. *J Urol* 184:913–917. <https://doi.org/10.1016/j.juro.2010.05.026>
 53. Brock M, von Bodman C, Palisaar RJ et al (2012) The impact of real-time elastography guiding a systematic prostate biopsy to improve cancer detection rate: a prospective study of 353 patients. *J Urol* 187:2039–2043. <https://doi.org/10.1016/j.juro.2012.01.063>
 54. Wang R, Chen J-J, Hu B (2015) Transrectal real-time elastography-guided transperineal prostate biopsy as an improved tool for prostate cancer diagnosis. *Int J Clin Exp Med* 8:6522–6529
 55. Tsutsumi M, Miyagawa T, Matsumura T et al (2007) The impact of real-time tissue elasticity imaging (elastography) on the detection of prostate cancer: clinicopathological analysis. *Int J Clin Oncol* 12:250–255. <https://doi.org/10.1007/s10147-007-0669-7>
 56. Kratzenberg J, Salomon G, Tennstedt P et al (2018) Prostate cancer rates in patients with initially negative elastography-targeted biopsy vs. systematic biopsy. *World J Urol* 36:623–628. <https://doi.org/10.1007/s00345-018-2178-x>
 57. Bercoff J, Tanter M, Fink M (2004) Supersonic shear imaging: a new technique for soft tissue elasticity mapping. *IEEE Trans Ultrason Ferroelectr Freq Control* 51:396–409. <https://doi.org/10.1109/tuffc.2004.1295425>
 58. Boehm K, Salomon G, Beyer B et al (2015) Shear wave elastography for localization of prostate cancer lesions and assessment of elasticity thresholds: implications for targeted biopsies and active surveillance protocols. *J Urol* 193:794–800. <https://doi.org/10.1016/j.juro.2014.09.100>
 59. Woo S, Kim SY, Lee MS et al (2015) Shear wave elastography assessment in the prostate: an intraobserver reproducibility study. *Clin Imaging* 39:484–487. <https://doi.org/10.1016/j.clinimag.2014.11.013>
 60. Woo S, Kim SY, Cho JY, Kim SH (2014) Shear wave elastography for detection of prostate cancer: a preliminary study. *Korean J Radiol* 15:346–355. <https://doi.org/10.3348/kjr.2014.15.3.346>
 61. Correas J-M, Tissier A-M, Khairoune A et al (2015) Prostate cancer: diagnostic performance of real-time shear-wave elastography. *Radiology* 275:280–289. <https://doi.org/10.1148/radiol.14140567>
 62. Ahmad S, Cao R, Varghese T et al (2013) Transrectal quantitative shear wave elastography in the detection and characterisation of prostate cancer. *Surg Endosc* 27:3280–3287. <https://doi.org/10.1007/s00464-013-2906-7>
 63. Rouvière O, Melodelima C, Hoang Dinh A et al (2017) Stiffness of benign and malignant prostate tissue measured by shear-wave elastography: a preliminary study. *Eur Radiol* 27:1858–1866. <https://doi.org/10.1007/s00330-016-4534-9>
 64. Barr RG, Memo R, Schaub CR (2012) Shear wave ultrasound elastography of the prostate: initial results. *Ultrasound Q* 28:13–20. <https://doi.org/10.1097/RUQ.0b013e318249f594>
 65. Ji Y, Ruan L, Ren W et al (2019) Stiffness of prostate gland measured by transrectal real-time shear wave elastography for detection

- of prostate cancer: a feasibility study. *Br J Radiol* 92:20180970. <https://doi.org/10.1259/bjr.20180970>
66. Boehm K, Budäus L, Tennstedt P et al (2015) Prediction of significant prostate cancer at prostate biopsy and per core detection rate of targeted and systematic biopsies using real-time shear wave elastography. *Urol Int* 95:189–196. <https://doi.org/10.1159/000431233>
 67. Xiang L-H, Fang Y, Wan J et al (2019) Shear-wave elastography: role in clinically significant prostate cancer with false-negative magnetic resonance imaging. *Eur Radiol* 29:6682–6689. <https://doi.org/10.1007/s00330-019-06274-w>
 68. Woo S, Suh CH, Kim SY et al (2017) Shear-wave elastography for detection of prostate cancer: a systematic review and diagnostic meta-analysis. *AJR Am J Roentgenol* 209:806–814. <https://doi.org/10.2214/AJR.17.18056>
 69. Yang Y, Zhao X, Zhao X et al (2019) Value of shear wave elastography for diagnosis of primary prostate cancer: a systematic review and meta-analysis. *Med Ultrason* 21:382–388. <https://doi.org/10.11152/mu-2051>
 70. Sidhu PS, Cantisani V, Dietrich CF et al (2018) The EFSUMB guidelines and recommendations for the clinical practice of contrast-enhanced ultrasound (CEUS) in non-hepatic applications: update 2017 (long version). *Ultraschall Med* 39:e2–e44. <https://doi.org/10.1055/a-0586-1107>
 71. Trabulsi EJ, Calio BP, Kamel SI et al (2019) Prostate contrast enhanced transrectal ultrasound evaluation of the prostate with whole-mount prostatectomy correlation. *Urology* 133:187–191. <https://doi.org/10.1016/j.urology.2019.07.026>
 72. Roy C, Buy X, Lang H et al (2003) Contrast enhanced color Doppler endorectal sonography of prostate: efficiency for detecting peripheral zone tumors and role for biopsy procedure. *J Urol* 170:69–72. <https://doi.org/10.1097/01.ju.0000072342.01573.8d>
 73. Mitterberger MJ, Aigner F, Horninger W et al (2010) Comparative efficiency of contrast-enhanced colour Doppler ultrasound targeted versus systematic biopsy for prostate cancer detection. *Eur Radiol* 20:2791–2796. <https://doi.org/10.1007/s00330-010-1860-1>
 74. Halpern EJ, Gomella LG, Forsberg F et al (2012) Contrast enhanced transrectal ultrasound for the detection of prostate cancer: a randomized, double-blind trial of dutasteride pretreatment. *J Urol* 188:1739–1745. <https://doi.org/10.1016/j.juro.2012.07.021>
 75. Yunkai Z, Yaqing C, Jun J et al (2019) Comparison of contrast-enhanced ultrasound targeted biopsy versus standard systematic biopsy for clinically significant prostate cancer detection: results of a prospective cohort study with 1024 patients. *World J Urol* 37:805–811. <https://doi.org/10.1007/s00345-018-2441-1>
 76. Li Y, Tang J, Fei X, Gao Y (2013) Diagnostic performance of contrast enhanced ultrasound in patients with prostate cancer: a meta-analysis. *Acad Radiol* 20:156–164. <https://doi.org/10.1016/j.acra.2012.09.018>
 77. Apfelbeck M, Chaloupka M, Schlenker B et al (2019) Follow-up after focal therapy of the prostate with high intensity focused ultrasound (HIFU) using contrast enhanced ultrasound (CEUS) in combination with MRI image fusion. *Clin Hemorheol Microcirc* 73:135–143. <https://doi.org/10.3233/CH-199222>
 78. Moschouris H, Stamatiou K, Malagari K et al (2019) The value of contrast-enhanced ultrasonography in detection of prostatic infarction after prostatic artery embolization for the treatment of symptomatic benign prostatic hyperplasia. *Diagn Interv Radiol Ank Turk* 25:134–143. <https://doi.org/10.5152/dir.2019.18410>
 79. Maxeiner A, Fischer T, Schwabe J et al (1980) (2019) Contrast-enhanced ultrasound (CEUS) and quantitative perfusion analysis in patients with suspicion for prostate cancer. *Ultraschall Med Stuttg Ger* 40:340–348. <https://doi.org/10.1055/a-0594-2093>
 80. Kuenen MPI, Saidov TA, Wijkstra H et al (2013) Spatiotemporal correlation of ultrasound contrast agent dilution curves for angiogenesis localization by dispersion imaging. *IEEE Trans Ultrason Ferroelectr Freq Control* 60:2665–2669. <https://doi.org/10.1109/TUFFC.2013.2865>
 81. van Sloun RJ, Demi L, Postema AW et al (2017) Ultrasound-contrast-agent dispersion and velocity imaging for prostate cancer localization. *Med Image Anal* 35:610–619. <https://doi.org/10.1016/j.media.2016.09.010>
 82. Postema AW, Frinking PJA, Smeenge M et al (2016) Dynamic contrast-enhanced ultrasound parametric imaging for the detection of prostate cancer. *BJU Int* 117:598–603. <https://doi.org/10.1111/bju.13116>
 83. Turco S, Frinking P, Wildeboer R et al (2020) Contrast-enhanced ultrasound quantification: from kinetic modeling to machine learning. *Ultrasound Med Biol*. <https://doi.org/10.1016/j.ultrasmedbio.2019.11.008>
 84. Kondo S, Takagi K, Nishida M et al (2017) Computer-aided diagnosis of focal liver lesions using contrast-enhanced ultrasonography with perflubutane microbubbles. *IEEE Trans Med Imaging* 36:1427–1437. <https://doi.org/10.1109/TMI.2017.2659734>
 85. Wildeboer RR, Postema AW, Demi L et al (2017) Multiparametric dynamic contrast-enhanced ultrasound imaging of prostate cancer. *Eur Radiol* 27:3226–3234. <https://doi.org/10.1007/s00330-016-4693-8>
 86. Palmeri ML, Glass TJ, Miller ZA et al (2016) Identifying clinically significant prostate cancers using 3-D in vivo acoustic radiation force impulse imaging with whole-mount histology validation. *Ultrasound Med Biol* 42:1251–1262. <https://doi.org/10.1016/j.ultrasmedbio.2016.01.004>
 87. Zhang M, Tang J, Luo Y et al (2019) Diagnostic performance of multiparametric transrectal ultrasound in localized prostate cancer: a comparative study with magnetic resonance imaging. *J Ultrasound Med Off J Am Inst Ultrasound Med* 38:1823–1830. <https://doi.org/10.1002/jum.14878>
 88. Rouvière O, Schoots IG, Mottet N (2019) Multiparametric magnetic resonance imaging before prostate biopsy: a chain is only as strong as its weakest link. *Eur Urol* 75:889–890. <https://doi.org/10.1016/j.eururo.2019.03.023>
 89. Wildeboer RR, Mannaerts CK, van Sloun RJG et al (2020) Automated multiparametric localization of prostate cancer based on B-mode, shear-wave elastography, and contrast-enhanced ultrasound radiomics. *Eur Radiol* 30:806–815. <https://doi.org/10.1007/s00330-019-06436-w>

Publisher's Note Springer Nature remains neutral with regard to jurisdictional claims in published maps and institutional affiliations.